Journal of the European Ceramic Society 38 (2018) 621–627

Contents lists available at ScienceDirect

Journal of the European Ceramic Society

journal homepage: www.elsevier.com/locate/jeurceramsoc

Original article

Origin of antipolar clusters in $BiFeO_3$ epitaxial thin films

Bin Liu[a,1], Chengpeng Yang[a,1], Xiaotian Li[a], Chao Wang[a], Guiju Liu[a], Huaiwen Yang[b], Yiqian Wang[a,*]

[a] College of Physics, Qingdao University, No. 308, Ningxia Road, Qingdao 266071, People's Republic of China
[b] Beijing National Laboratory for Condensed Matter Physics, Institute of Physics, Chinese Academy of Sciences, Beijing 100080, People's Republic of China

ARTICLE INFO

Keywords:
$BiFeO_3$ film
Modulated structure
Antiparallel cation displacements

ABSTRACT

The microstructure of $BiFeO_3$ (BFO) thin films is investigated using high-resolution transmission electron microscopy. Both (001)- and (101)-type domain boundaries are found in the BFO films. The antipolar clusters induced by antiparallel cation displacements are observed in the pure BFO film, and the cation displacements in the films are proved to originate from the lattice strain which can be adjusted by introduction of a buffer layer. Combining transmission electron microscopy (TEM) with fast Fourier transformation techniques, both γ-Fe_2O_3 and FeO phases were discovered. The γ-Fe_2O_3 phase stems from the decomposition of stoichiometric BFO due to the volatilization of Bi, while the FeO phase results from the decomposition of BFO with oxygen vacancies which could come from ion milling process during the TEM sample preparation. Our work sheds light on the origin of the cation displacements and provides a new idea to control the physical properties of BFO films.

1. Introduction

Bismuth ferrite $BiFeO_3$ (BFO) films have attracted a great deal of attention in recent years [1–5] owing to their excellent physical properties. The excellent properties are indispensable for their applications in electronic devices such as sensors, micro actuators, infrared detectors, microwave phase filters and ultimately non-volatile memories [6–10]. BFO has been identified as an environmentally friendly alternative to current lead-based piezoelectrics. However, the small magnetization and narrow growth window of BFO impede its practical applications. To overcome the aforementioned shortcomings and improve its property, A- and/or B-site doping of the BFO has been attempted [11–15].

In 1951, the antiparallel cation (Pb^{3+}) displacements were firstly discovered in $PbZrO_3$ [16] and the symmetry of displacement was confirmed by electron diffraction patterns [17,18]. Until 2008, Cheng et al. [19,20] observed the antiferroelectric local antipolar clusters induced by the antiparallel cation displacements in Sm-doped BFO films, which was attributed to the Sm doping. To date, the origin of cation displacements remains controversial. In this work, we observed antipolar clusters with same features in the pure BFO films using TEM, which is thought to originate from the lattice strain imposed by the substrate.

In the BFO films prepared by pulsed laser deposition (PLD), the coexistence of α-Fe_2O_3, γ-Fe_2O_3 and parent BFO phases has been reported in previous literature [21,22]. The presence of these phases can substantially affect the electrical and magnetic properties of the whole material [23]. In our work, apart from the γ-Fe_2O_3 precipitate, FeO phase is observed in the BFO film.

2. Experimental details

The 380-nm BFO film was fabricated on (001) $SrTiO_3$ (STO) substrate and the 40-nm BFO film was prepared on (001) $LaAlO_3$ (LAO) substrate using PLD technique. During the deposition, the substrates were maintained at 750 °C and the oxygen pressures at 15 Pa. The laser wavelength was 248 nm, the pulse fluence was 1.5 J/cm^2, and the ablation frequency was 1 Hz. After deposition, the films were cooled to room temperature under the deposition pressure. To tune the strain state of BFO film, a bi-layer thin-film heterostructures of BFO (380 nm)/$La_{0.5}Ca_{0.5}MnO_3$ (LCMO, 50 nm) and the BFO (40 nm)/$La_{0.5}Sr_{0.5}MnO_3$ (LSMO, 10 nm) were deposited on STO and LAO, respectively.

Specimens for TEM examinations were prepared in cross-sectional orientations ([010] zone axis of STO and LAO substrates) using conventional techniques of mechanical polishing and ion thinning. The ion milling was performed using a Gatan model 691 precision ion polishing system (PIPS). The bright-field (BF) imaging, selected-area electron diffraction (SAED), and high-resolution TEM (HRTEM) examinations were carried out on a JEOL JEM2100F electron microscope operated at

* Corresponding author.
E-mail address: yqwang@qdu.edu.cn (Y. Wang).
[1] These authors contributed equally to this work.

http://dx.doi.org/10.1016/j.jeurceramsoc.2017.09.041
Received 10 July 2017; Received in revised form 19 September 2017; Accepted 25 September 2017
Available online 28 September 2017
0955-2219/

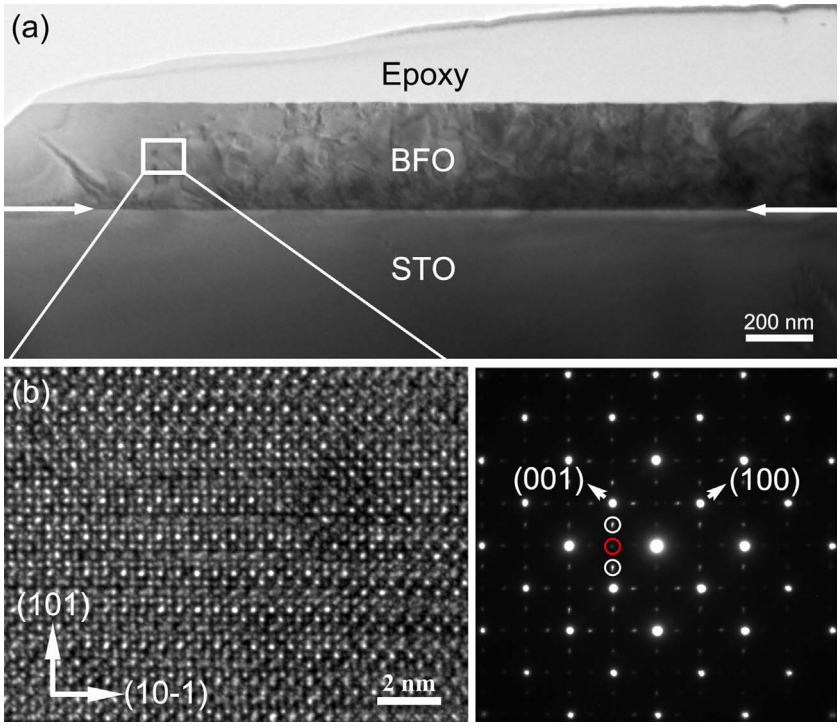

Fig. 1. (a) Cross-sectional BF image of BFO/STO film; Typical HRTEM image (b) and SAED pattern (c) of the enclosed region.

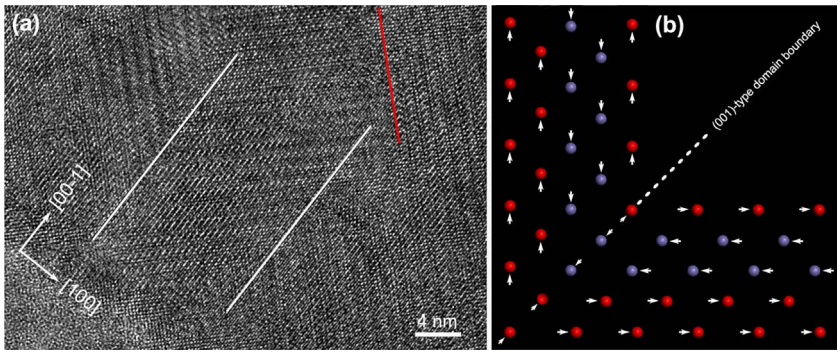

Fig. 2. (a) A cross-sectional [010] zone axis HRTEM image of BFO showing the (001)- and (101)-type domain boundaries; (b) The projected atom arrangements at the boundary. The red and blue circles represent Bi atoms with antiparallel displacements, respectively. (For interpretation of the references to color in this figure legend, the reader is referred to the web version of this article.)

200 kV. The chemical compositions of BFO films grown on different substrates were determined using energy dispersive x-ray spectroscopy (EDS) in a JEOL JEM2100F TEM, which shows that all the epitaxial films are pure BFO. The film structure was analyzed by x-ray diffraction (Bruker x-ray diffractometer, $\lambda = 1.5406$ Å).

3. Results and discussion

Fig. 1(a) shows a cross-sectional BF image of BFO/STO film. The interface between the film and the substrate is labeled by white arrows. From this BF image we can see that the BFO film is homogeneous and has a smooth surface. To study its microstructure, extensive HRTEM examinations are performed. A great number of modulated structures are found in this film and a typical one is shown in Fig. 1(b). Modulated bright and dark stripes with a periodicity (~11.27 Å) of two-fold the original (101) lattice distance can be found in this image. To investigate the origin of these modulated structures, the SAED technique is adopted and the results are shown in Fig. 1(c). It is obvious that in addition to the fundamental reflections, superlattice diffraction spots are observed in the SAED pattern, which are located at half or quarter positions between fundamental {101} reflections. The wave vectors of these spots are $[\frac{1}{2}00]$ (red circle) or $[\frac{1}{4}00]$ (white circles), which represent the modulated structures with a periodicity twice or fourfold the original lattice parameter. This image shows a remarkable resemblance to ⟨010⟩ SAED patterns from the well-established antiferroelectric system of $PbZr_xTi_{1-x}O_3$ [17,18], in which the antipolar phases were proved to arise from condensation of two phonon modes, *i.e.*, condensation of the$(\frac{1}{2}\frac{1}{2}0)(\pi/a)\sum_3$ corresponding to $\frac{1}{4}\{011\}$ reflections (white circles); condensation of $(110)(\pi/a)M_5$ corresponding to $\frac{1}{2}\{011\}$ reflections (red circles). In analogy to the previous literature, the $\frac{1}{4}\{011\}$ reflections in SAED patterns of BFO film come from the antiparallel cation (Bi^{3+}) displacement and the $\frac{1}{2}\{011\}$ ones are directly associated with the antiphase tilting of oxygen octahedra [19,20,24]. Therefore, Sm-doping [19] is certainly not the origin of the cation displacement because similar features are observed in the BFO films without doping.

The pseudocubic BFO can produce domain structures in the epitaxial films. The typical domain boundaries in BFO are (001) and (101), labeled by white and red lines in Fig. 2(a), respectively. Based on the antiparallel cation displacement model [16], the projected atom arrangements at the boundary can be determined, as shown in Fig. 2(b).

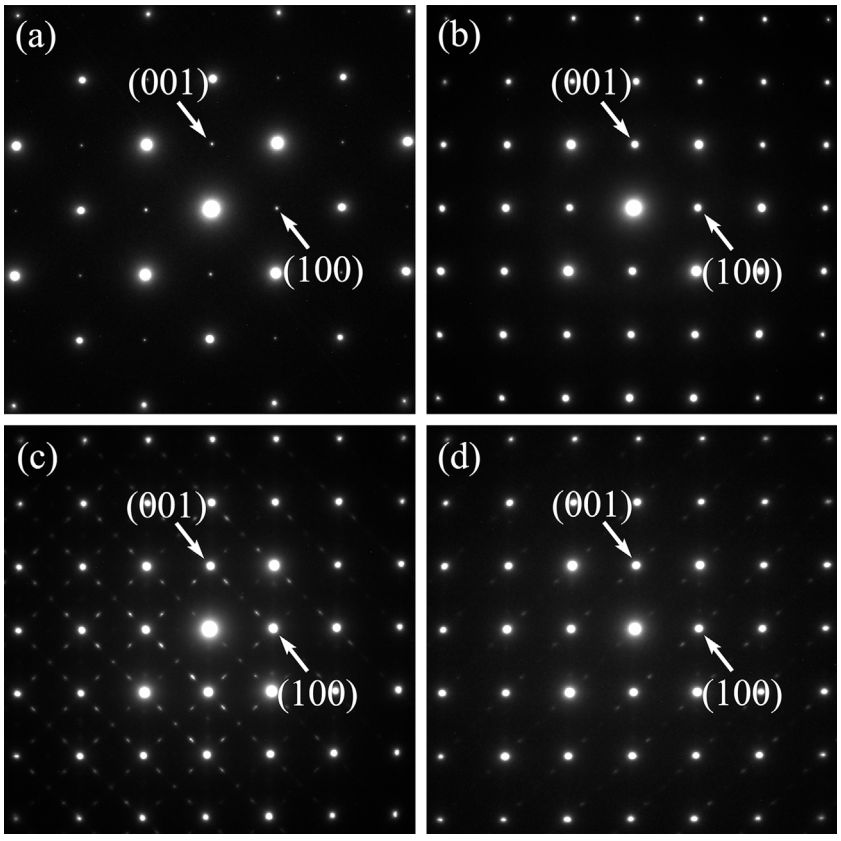

Fig. 3. (a) Typical SAED pattern of STO substrate; (b)–(d) Typical SAED pattern taken from BFO films at a distance of about 50, 150, 250 nm from the interface.

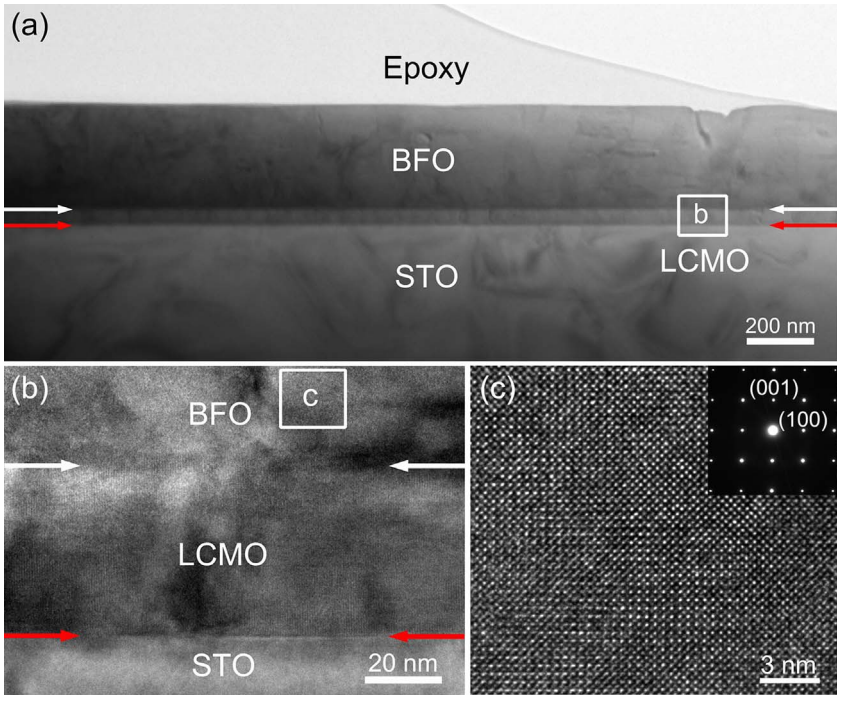

Fig. 4. (a) Cross-sectional BF image of BFO/STO film with a buffer layer of LCMO; (b) Enlarged image of the enclosed region in (a); (c) Typical HRTEM image of the enclosed region in (b). The inset shows the SAED pattern of BFO film.

The two adjacent domains are rotated with an angle of 90°. It can be seen from the image that the elements meeting at the interface develop a small antiparallel displacements along [001]. A (001)-type domain boundary is indicated by dashed lines. This structural model satisfies the symmetry of both domains.

Fig. 3(a) shows the SAED pattern of STO substrate, and Fig. 3(b–d) are the SAED patterns taken from different regions of BFO film. The lattice parameters of the film and the substrate can be calculated from the SAED patterns. From the regions away from the interface at a distance of 50, 150 and 250 nm, a changes from 3.988 Å to 3.994 Å and

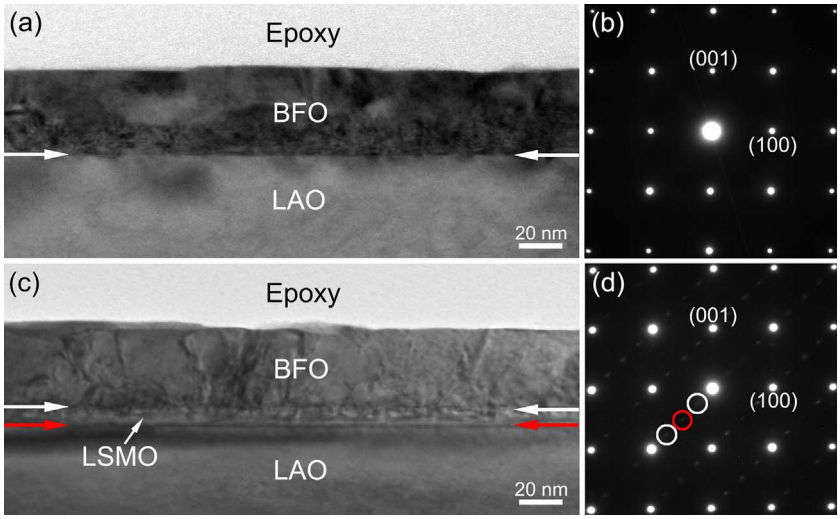

Fig. 5. Cross-sectional BF image (a) and the SAED pattern (b) of BFO film grown on LAO; Corresponding BF image (c) and SAED pattern (d) of BFO/LAO film with a buffer layer of LSMO.

4.000 Å, and *c* changes from 4.019 Å to 4.009 Å and 4.004 Å. In the region close to the interface (< 50 nm), the compressive strain from the substrate is strong and no superlattice diffraction spots appear in the SAED pattern. In the central region (from 50 to 150 nm), one can see the superlattice diffraction spots induced by the antiparallel cation displacement. However, in the region far from the interface (> 250 nm), the superlattice diffraction spots fade away. In other words, there is a strain gradient in the BFO film from the interface to the free surface of the film, and the antiparallel cation displacement only happens in a narrow strain range. It is consistent with the fact that the chemical arrangement can be tuned by epitaxial strain imposed by the substrate [25,26]. To clarify whether the epitaxial strain plays a significant role in the antiparallel displacement of the A-sites cations, BFO/STO film with a buffer layer of LCMO is investigated using TEM in details and the results are shown in Fig. 4. Compared with Fig. 1(a), except the buffer layer, no obvious difference can be found in this BF image [Fig. 4(a)]. From the enlarged interface image in Fig. 4(c), it can be seen that the buffer layer has a good epitaxial relationship between BFO film and STO substrate. Compared with BFO/STO film, the difference is that no antipolar clusters can be found in this HRTEM image. Certainly, no $\frac{1}{4}\{011\}$ or $\frac{1}{2}\{011\}$ reflections, which can indicate antiparallel cation displacements and antiphase tilting of oxygen octahedra, can be found in the SAED pattern [insets in Fig. 4(c)]. In other words, when a buffer layer of LCMO is introduced between BFO film and STO substrate, the cation antiparallel displacements just disappear. Thus, we deduce that the epitaxial strain provided by the STO substrate induces the antiparallel cation displacements. The lattice parameter of BFO (3.952 Å) is larger than that of STO (3.905 Å) and much larger than that of LCMO (3.831 Å), so the inserted buffer layer greatly influences the strain state of BFO film, which results in the disappearance of the cation displacements. To verify this conclusion, BFO/LAO and BFO/LSMO/LAO films are also studied and the TEM results are shown in Fig. 5. In the BFO/LAO film, no $\frac{1}{4}\{011\}$ or $\frac{1}{2}\{011\}$ superlattice reflections can be found, which indicates that no cation displacement takes place. However, when the buffer layer LSMO is introduced, the weak $\frac{1}{4}\{101\}$ and $\frac{1}{2}\{101\}$ reflections appear, which indicates that a small amount of antipolar clusters forms. Either tensile or compressive stress can induce the antiparallel cation displacement, but it is only in a narrow range. The inserted LSMO layer relieves the compressive stress from the substrate and thus the cations cannot displace antiparallel again. Cheng et al. [19,20] investigated the microstructure of BFO films with different doping contents of Sm, and found that the antipolar clusters begin to appear at a doping content of ~8%, which grow with the increase of Sm doping content. As we all know, the ionic radii of Bi^{3+} and Sm^{3+} are different. Thus, it is the doped Sm^{3+} that changes the strain state of the films and results in the cation displacement. The antipolar clusters only form in a small doping range, which just verifies our conclusion that cation displacements only form in a narrow strain range and Sm^{3+} itself does not play a direct role in the cation displacement.

In addition to the above results, a number of precipitates are observed in the BFO/LAO film. In the HRTEM image shown in Fig. 6(a), the precipitate phase is circled by white lines at the interface. To clarify the nature of this phase, fast Fourier transformation (FFT) is employed and the result is shown in Fig. 6(b). In this image, except the fundamental perovskite reflections from the parent BFO lattice, another set of dots (in red circles) is observed. From these reflections, we can deduce that it is a typical [110] zone-axis diffraction pattern from a cubic phase. The inverse FFT (IFFT) is also performed and the result is demonstrated in Fig. 6(c). In this image, the lattice spacings of (220) and (200) planes are measured to be 2.96 and 4.18 Å, respectively, which are consistent with the lattice parameters of γ-Fe_2O_3. Thus, we conclude that this circled precipitate phase is γ-Fe_2O_3. Interestingly, Moire fringes are observed in the BFO/LAO film as shown in Fig. 7(a) and its FFT results are shown in Fig. 7(b). In addition to the fundamental reflections (in white circles), additional dots (in red circles) are also observed. The corresponding IFFT results are shown in Fig. 7(b) and (c), respectively. From the measured lattice distances, we confirm that the planes in Fig. 7(c) correspond to (110) planes of BFO and those in Fig. 7(d) are (200) planes of FeO. The IFFT results of both sets of reflections in white and red circles are enclosed in Fig. 7(b), which are consistent with the experimental HRTEM image. Thus, it is suggested that the Moire fringes come from the interference between the lattices of parent BFO and FeO precipitate. Because FeO is unstable and can be easily oxidized into Fe_2O_3, it is difficult to directly observe the FeO phase in BFO film. What's more, we find that all the γ-Fe_2O_3 phases are located at the interface between BFO film and LAO substrate. On the contrary, all the FeO phases are far away from the interface. In the experimental details, we mentioned that the specimens were prepared using argon ion thinning. In the milling process, oxygen atoms near the film surface are more likely to be removed from the film than those near the interface. We believe that both γ-Fe_2O_3 and FeO phases come from the volatilization of Bi. The BFO with oxygen vacancies is decomposed into Bi_2O_3 and FeO, and that without oxygen vacancies is turned into Bi_2O_3 and γ-Fe_2O_3. That is why all the γ-Fe_2O_3 phases are located at the interface and all the FeO phases are far away from it. To verify our

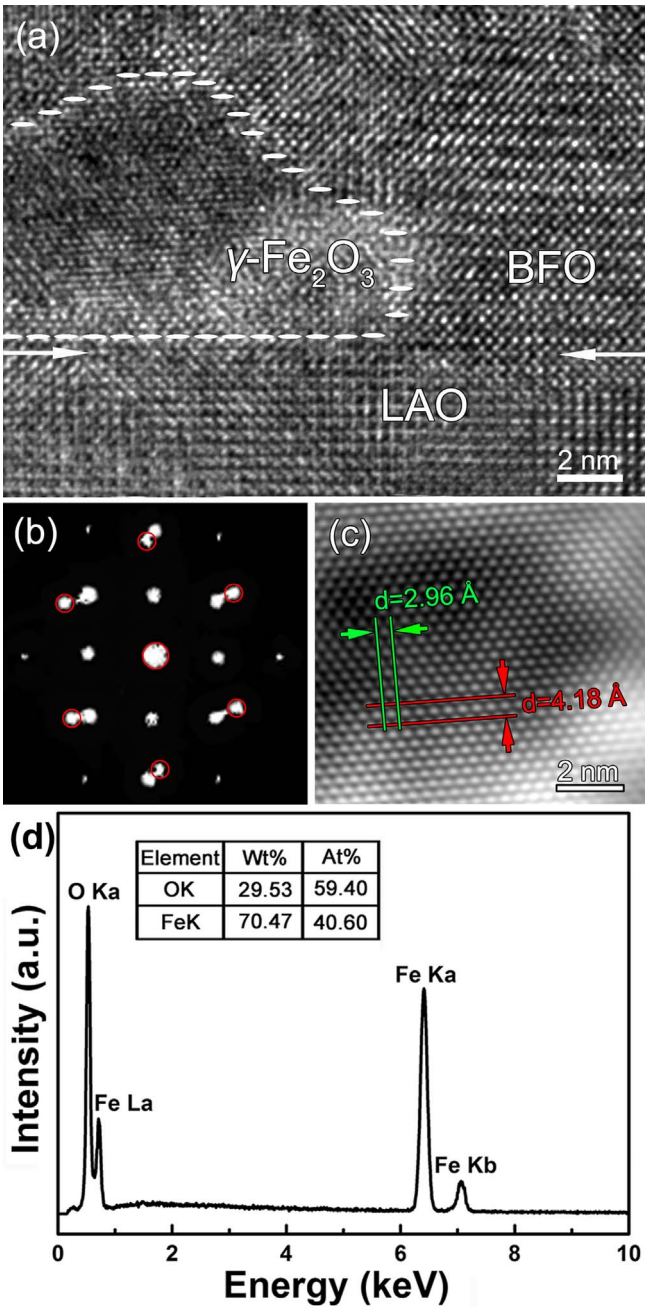

Fig. 6. HRTEM image (a) of BFO/LAO film and its FFT (b); (c) IFFT of the reflections in the red circles; (d) Typical EDS spectrum of γ-Fe_2O_3. (For interpretation of the references to color in this figure legend, the reader is referred to the web version of this article.)

conclusion, the film is investigated by x-ray diffraction (XRD) and the results are shown in Fig. 8. All the diffraction peaks of Bi_2O_3, γ-Fe_2O_3, parent BFO and LAO substrate can be found in this pattern. However, no diffraction peak of FeO can be detected. Because the XRD analysis is performed before the TEM examination, the oxygen atoms are not removed from the BFO film. In this case, all the BFO is converted into Bi_2O_3 and γ-Fe_2O_3 without formation of FeO phases.

4. Conclusion

The microstructure of BFO films grown on two different substrates is systematically studied. In the pure BFO film grown on STO, two types of domain boundaries are found, and the antipolar clusters induced by antiparallel cation displacements are also observed. Through changing the substrate or introducing a buffer layer, it is concluded that the cation displacements are induced by the epitaxial strain which can be tuned by introduction of a buffer layer. Combining TEM with FFT (and

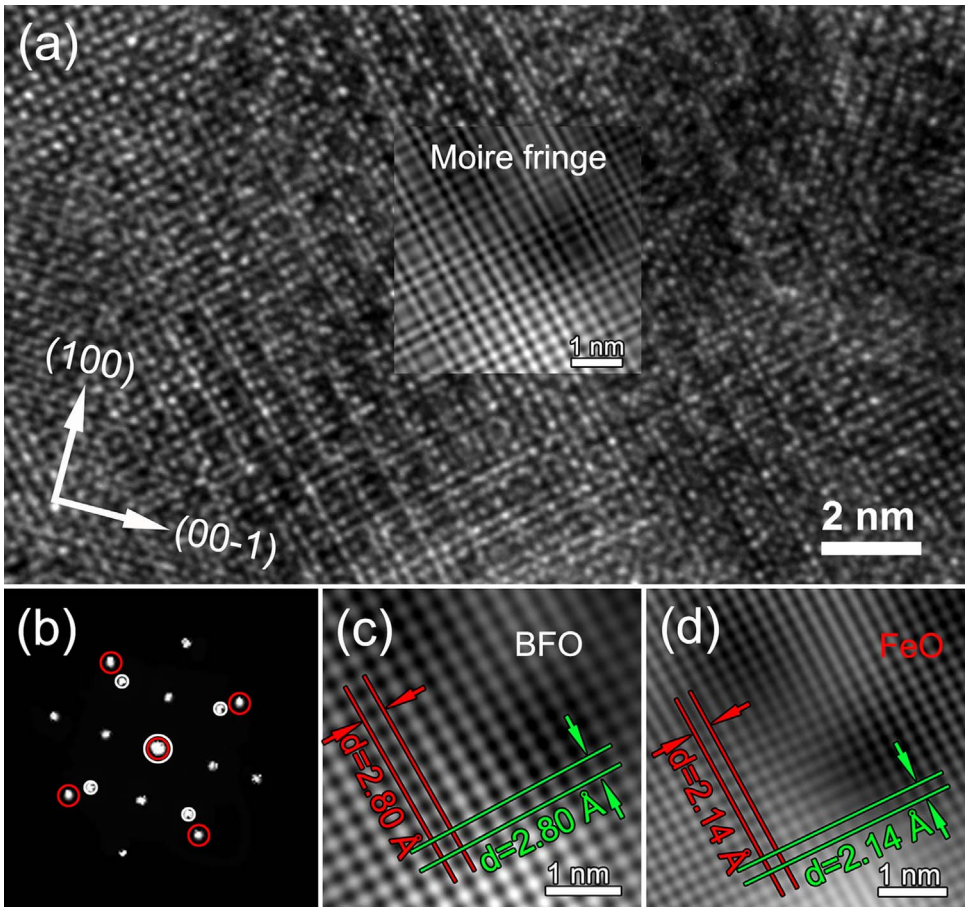

Fig. 7. HRTEM image (a) of BFO/LAO film and its FFT (b); IFFT of the reflections in the red circles (c) and in the white (d); The inset shows the IFFT of all the reflections. (For interpretation of the references to color in this figure legend, the reader is referred to the web version of this article.)

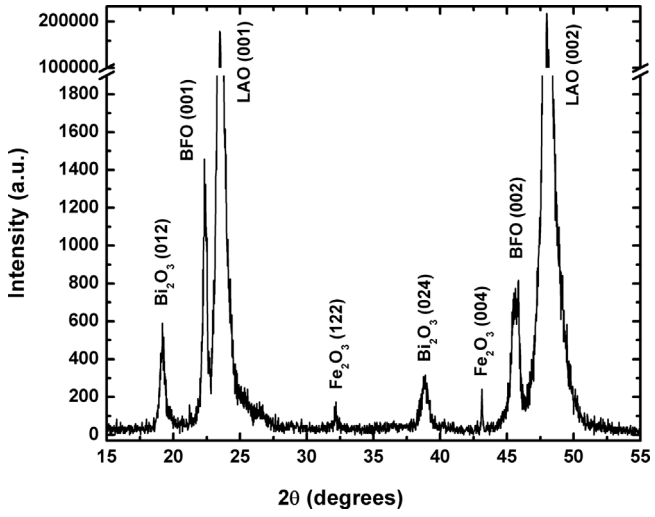

Fig. 8. XRD pattern of BFO/LAO film.

IFFT) techniques, the γ-Fe_2O_3 and FeO phases are discovered in the BFO film grown on LAO. Due to the volatilization of Bi, the BFO with oxygen vacancies is converted into Bi_2O_3 and FeO, and that without oxygen vacancies is transformed into Bi_2O_3 and γ-Fe_2O_3.

Acknowledgments

We would like to thank the financial support from the National Key Basic Research Development Program of China (Grant Nos.: 2012CB722705, 2013CB921700), the National Natural Science Foundation of China (Grant Nos.: 10974105 and 11520101002), and High-end Foreign Experts Recruitment Programs (Grant Nos.: GDW20143500163, GDW20163500110). Y. Q. Wang would also like to thank the financial support from the Taishan Scholar Program of Shandong Province, the Top-notch Innovative Talent Program of Qingdao City (Grant No.: 13-CX-08), and Qingdao International Center for Semiconductor Photoelectric Nanomaterials.

References

[1] B. Marchand, P. Jalkanen, V. Tuboltsev, M. Vehkamaki, M. Puttaswamy, M. Kemell, K. Mizohata, T. Hatanpaa, A. Savin, J. Raisanen, M. Ritala, M. Leskela, Electric and magnetic properties of ALD-grown $BiFeO_3$ films, J. Phys. Chem. C 120 (2016) 7313–7322.
[2] Y.R. Yang, W. Ren, M. Stengel, X.H. Yan, L. Bellaiche, Revisiting properties of ferroelectric and multiferroic thin films under tensile strain from first principles, Phys. Rev. Lett. 109 (2012) 057602.
[3] S.M. He, G.L. Liu, D.P. Zhu, S.S. Kang, Y.X. Chen, S.S. Yan, L.M. Mei, Structural and physical properties of $BiFeO_3$ thin films epitaxially grown on $SrTiO_3$ (001) and polar (111) surfaces, Chin. Phys. B 23 (2014) 036801.
[4] A.F. Popkov, M.D. Davydova, K.A. Zvezdin, S.V. Solov'yov, A.K. Zvezdin, Origin of the giant linear magnetoelectric effect in perovskitelike multiferroic $BiFeO_3$, Phys. Rev. B 93 (2016) 094435.
[5] H. Béa, M. Bibes, S. Fusil, K. Bouzehouane, E. Jacquet, K. Rode, P. Bencok, A. Barthélémy, Investigation on the origin of the magnetic moment of $BiFeO_3$ thin films by advanced x-ray characterizations, Phys. Rev. B 74 (2006) 020101(R).
[6] G. Catalan, J.F. Scott, Physics and applications of bismuth ferrite, Adv. Mater. 21 (2009) 2463–2485.
[7] K.F. Wang, J.M. Liu, Z.F. Ren, Multiferroicity: the coupling between magnetic and polarization orders, Adv. Phys. 58 (2009) 321–448.
[8] S.Y. Yang, J. Seidel, S.J. Byrnes, P. Shafer, C.H. Yang, M.D. Rossell, P. Yu, Y.H. Chu, J.F. Scott, J.W. Ager, L.W. Martin, R. Ramesh, Above-bandgap voltages from ferroelectric photovoltaic devices, Nat. Nanotechnol. 5 (2010) 143–147.
[9] J. Ma, J.M. Hu, Z. Li, C.W. Nan, Recent progress in multiferroic magnetoelectric composites: from bulk to thin films, Adv. Mater. 23 (2011) 1062–1087.
[10] S. Hong, T. Choi, J.H. Jeon, Y. Kim, H. Lee, H.Y. Joo, I. Hwang, J.S. Kim, S.O. Kang, S.V. Kalinin, B.H. Park, Large resistive switching in ferroelectric $BiFeO_3$ nano-island based switchable diodes, Adv. Mater. 25 (2013) 2339–2343.
[11] Y.H. Chu, Q. Zhan, C.H. Yang, M.P. Cruz, L.W. Martin, T. Zhao, P. Yu, R. Ramesh, P.T. Joseph, I.N. Lin, W. Tian, D.G. Schlom, Low voltage performance of epitaxial $BiFeO_3$ films on Si substrates through lanthanum substitution, Appl. Phys. Lett. 92

(2008) 102909.
[12] G.L. Yuan, S.W. Or, Multiferroicity in polarized single-phase $Bi_{0.875}Sm_{0.125}FeO_3$ ceramics, J. Appl. Phys. 100 (2006) 024109.
[13] H.Y. Dai, T. Li, Z.P. Chen, D.W. Liu, R.Z. Xue, C.Z. Zhao, H.Z. Liu, N.K. Huang, Studies on the structural, electrical and magnetic properties of Ce-doped $BiFeO_3$ ceramics, J. Alloys Compd. 672 (2016) 182–189.
[14] H. Izumi, T. Yoshimura, N. Fujimura, Growth and ferroelectric properties of La and Al codoped $BiFeO_3$ epitaxial films, J. Appl. Phys. 121 (2017) 174102.
[15] K.T. Liu, J. Li, J.B. Xu, F.L. Xu, L. Wang, L. Bian, Study on dielectric, optic and magnetic properties of manganese and nickel co-doped bismuth ferrite thin film, J. Mater. Sci: Mater. Electron. 28 (2017) 5609–5614.
[16] E. Sawaguchi, H. Maniwa, S. Hoshino, Antiferroelectric structure of lead zirconate, Phys. Rev. 83 (1951) 1078.
[17] D.I. Woodward, J. Knudsen, I.M. Reaney, Review of crystal and domain structures in the $PbZr_xTi_{1-x}O_3$ solid solution, Phys. Rev. B 72 (2005) 104110.
[18] D. Viehland, Transmission electron microscopy study of high-Zr-content lead zirconate titanate, Phys. Rev. B 52 (1995) 778–791.
[19] C.J. Cheng, D. Kan, S.H. Lim, W.R. McKenzie, P.R. Munroe, L.G. Salamanca-Riba, R.L. Withers, I. Takeuchi, V. Nagarajan, Structural transitions and complex domain structures across a ferroelectric-to-antiferroelectric phase boundary in epitaxial Sm-doped $BiFeO_3$ thin films, Phys. Rev. B 80 (2009) 014109.
[20] C.J. Cheng, A.Y. Borisevich, D. Kan, I. Takeuchi, V. Nagarajan, Nanoscale structural and chemical properties of antipolar clusters in Sm-doped $BiFeO_3$ ferroelectric epitaxial thin films, Chem. Mater. 22 (2010) 2588–2596.
[21] S.H. Lim, M. Murakami, W.L. Sarney, S.Q. Ren, The effects of multiphase formation on strain relaxation and magnetization in multiferroic $BiFeO_3$ thin films, Adv. Funct. Mater. 17 (2007) 2594–2599.
[22] H. Béa, M. Bibes, A. Barthélémy, K. Bouzehouane, E. Jacquet, A. Khodan, J.P. Contour, S. Fusil, F. Wyczisk, A. Forget, D. Lebeugle, D. Colson, M. Viret, Influence of parasitic phases on the properties of $BiFeO_3$ epitaxial thin films, Appl. Phys. Lett. 87 (2005) 072508.
[23] M. Murakami, S. Fujino, S.H. Lim, L.G. Salamanca-Riba, M. Wuttig, I. Takeuchi, B. Varughese, H. Sugaya, T. Hasegawa, S.E. Lofland, Microstructure and phase control in Bi-Fe-O multiferroic nanocomposite thin films, Appl. Phys. Lett. 88 (2006) 112505.
[24] Z.Y. Liao, F. Xue, W. Sun, D.S. Song, Q.Q. Zhang, J.F. Li, L.Q. Chen, J. Zhu, Reversible phase transition induced large piezoelectric response in Sm-doped $BiFeO_3$ with a composition near the morphotropic phase boundary, Phys. Rev. B 95 (2017) 214101.
[25] W. Donner, C.L. Chen, M. Liu, A.J. Jacobson, Y.L. Lee, M. Gadre, D. Morgan, Epitaxial strain-induced chemical ordering in $La_{0.5}Sr_{0.5}CoO_{3-\delta}$ films on $SrTiO_3$, Chem. Mater. 23 (2011) 984–988.
[26] P.S.S.R. Krishnan, A.N. Morozovska, E.A. Eliseev, Q.M. Ramasse, D. Kepaptsoglou, W.I. Liang, Y.H. Chu, P. Munroe, V. Nagarajan, Misfit strain driven cation interdiffusion across an epitaxial multiferroic thin film interface, J. Appl. Phys. 115 (2014) 054103.